Monthly Notices
of the
ROYAL ASTRONOMICAL SOCIETY

MNRAS **453,** 4037–4050 (2015) doi:10.1093/mnras/stv1845

Investigating powerful jets in radio-loud narrow-line Seyfert 1s

M. Orienti,[1⋆] F. D'Ammando,[1,2] J. Larsson,[3] J. Finke,[4] M. Giroletti,[1] D. Dallacasa,[1,2] T. Isacsson[3] and J. Stoby Hoglund[3]

[1]*INAF – Istituto di Radioastronomia, via Gobetti 101, I-40129 Bologna, Italy*
[2]*Dipartimento di Fisica e Astronomia, Universià degli Studi di Bologna, via Ranzani 1, I-40127 Bologna, Italy*
[3]*KTH, Department of Physics, and the Oskar Klein Centre, AlbaNova, SE-106 91 Stockholm, Sweden*
[4]*US Naval Research Laboratory, Code 7653, 4555 Overlook Avenue SW, Washington, DC 20375-5352, USA*

Accepted 2015 August 7. Received 2015 August 3; in original form 2015 June 5

ABSTRACT

We report results on multiband observations from radio to γ-rays of the two radio-loud narrow-line Seyfert 1 (NLSy1) galaxies PKS 2004−447 and J1548+3511. Both sources show a core–jet structure on parsec scale, while they are unresolved at the arcsecond scale. The high core dominance and the high variability brightness temperature make these NLSy1 galaxies good γ-ray source candidates. *Fermi*-Large Area Telescope detected γ-ray emission only from PKS 2004−447, with a γ-ray luminosity comparable to that observed in blazars. No γ-ray emission is observed for J1548+3511. Both sources are variable in X-rays. J1548+3511 shows a hardening of the spectrum during high activity states, while PKS 2004−447 has no spectral variability. A spectral steepening likely related to the soft excess is hinted below 2 keV for J1548+3511, while the X-ray spectra of PKS 2004−447 collected by *XMM–Newton* in 2012 are described by a single power law without significant soft excess. No additional absorption above the Galactic column density or the presence of an Fe line is detected in the X-ray spectra of both sources.

Key words: galaxies: active – galaxies: Seyfert – gamma-rays: general – radio continuum: general.

1 INTRODUCTION

Narrow-line Seyfert 1 (NLSy1) galaxies represent a rare type of classical Seyfert galaxies. The strong featureless X-ray continuum and the strong high-ionization lines shown by NLSy1 are common in Seyfert 1. However, the optical permitted emission lines are narrow, i.e. more similar to Seyfert 2 galaxies, indicating a combination of properties from both types. Their optical spectra are characterized by narrow permitted lines (full width at half-maximum, FWHM $\leq$ 2000 km s^{-1}), weak [O III]/λ5007 emission line ([O III]/Hβ $<$ 3), and usually strong Fe II emission lines (Osterbrock & Pogge 1985).

NLSy1 are usually hosted in spiral galaxies, although some objects are associated with early-type S0 galaxies (see e.g. Mrk 705 and Mrk 1239; Markarian et al. 1989).

Extreme characteristics are observed in the X-ray band, where strong and rapid variability is observed more frequently than in classical Seyfert 1. The X-ray spectrum of NLSy1 is usually described by a power law which dominates in the 2–10 keV energy range, and a soft X-ray excess at lower energies. The X-ray spectrum between 0.3 and 10 keV is steeper than in Seyfert 1 (Grupe et al. 2010), while the photon index of the hard X-ray spectrum is similar (Panessa et al. 2011). The complex X-ray spectrum is interpreted in terms of either relativistic blurred disc reflection, or ionized/neutral absorption covering the X-ray source (Fabian et al. 2009; Miller et al. 2010).

About 7 per cent of NLSy1 are radio-loud (RL), with a smaller fraction ($\sim$2.5 per cent) exhibiting a high radio loudness parameter[1] (R > 100; Komossa et al. 2006). In the radio band, RL-NLSy1 usually show a compact morphology with a one-sided jet emerging from the bright core and extending up to a few parsecs. In some objects the radio emission extends on kpc scales (Antón, Browne & Marcha 2008; Doi et al. 2012; Richards & Lister 2015). The high values of both brightness temperature and core dominance suggest the presence of non-thermal emission from relativistic jets (Doi, Asada & Nagai 2011). The measurement of superluminal motion in the RL-NLSy1 SBS 0846+513 indicates Doppler boosting effects in relativistic jets (D'Ammando et al. 2013b). It is worth noting that some evidence of pc-scale jet-like structure is also found in some radio-quiet (RQ) NLSy1, but the nature of the outflow is still under debate (e.g. Doi et al. 2013).

⋆ E-mail: orienti@ira.inaf.it

[1] The radio loudness is defined as the ratio between the radio flux density at 6 cm and the optical B-band flux (Kellermann et al. 1989).

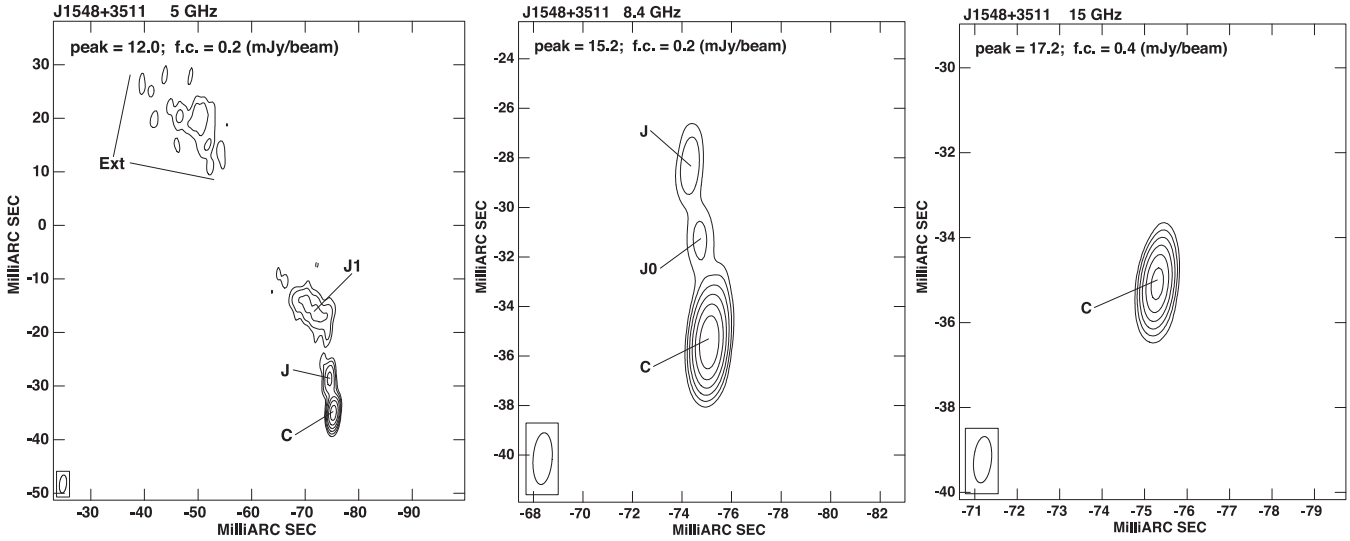

Figure 1. VLBA images of J1548+3511 at 5 GHz (left), 8.4 GHz (centre), and 15 GHz (right). On each image we provide the peak flux density in mJy beam^{-1} and the first contour intensity (f.c.) in mJy beam^{-1}, which corresponds to three times the off-source noise level measured on the image plane. Contours increase by a factor of 2. The restoring beam is plotted in the bottom left-hand corner of each panel.

Strong evidence in favour of highly relativistic jets in RL-NLSy1 is the detection by the Large Area Telescope (LAT) on-board the *Fermi* satellite of γ-ray emission from six RL-NLSy1: PMN J0948+0022, 1H 0323+342, PKS 1502+036, PKS 2004−447 (Abdo et al. 2009), SBS 0846+513 (D'Ammando et al. 2012), and FBQS J1644+2619 (D'Ammando et al. 2015b). The γ-ray emission is variable, showing flaring activity accompanied by a moderate hardening of the spectrum. The peculiar multiwavelength properties together with the γ-ray flares make the RL-NLSy1 more similar to blazars rather than classical Seyfert galaxies, at least at high energies.

Relativistic jets produced by nuclear objects which are thought to be hosted mainly in spiral galaxies are somehow puzzling. RL-NLSy1 are usually found at higher redshift than RQ-NLSy1 and no optical morphological studies have been carried out so far, with the exception of 1H 0323+342. The optical morphology of the host galaxy is compatible with either a one-armed spiral (Zhou et al. 2007) or a ring-like structure produced by a recent merger (Antón et al. 2008; León-Tavares et al. 2014).

In this paper we present results of a multiwavelength study, from radio to γ-rays, of the RL-NLSy1 J1548+3511 and PKS 2004−447. J1548+3511 is a NLSy1 at redshift $z = 0.478$ with a radio loudness $R \sim 110$ and an estimated black hole (BH) mass $M_{\rm BH} = 10^{7.9}$ M$_\odot$ (Yuan et al. 2008), while PKS 2004−447, at redshift $z = 0.24$, has $1710 < R < 6320$ and the estimated BH mass $M_{\rm BH} = 10^{6.7}$ M$_\odot$ (Oshlack, Webster & Whiting 2001). These sources have been selected on the basis of their high variability brightness temperature $T'_{\rm B,var} = 10^{13}$–10^{15} K that is considered a good indicator for the presence of Doppler boosting in relativistic jets. Among the RL-NLSy1 presented in the sample by Yuan et al. (2008), J1548+3511 is the only source with $T'_{\rm B,var}$ as high as those found in γ-ray-loud NLSy1. However, no γ-ray emission has been detected from this source so far. In this paper we aim at investigating differences and similarities between the γ-ray emitter PKS 2004−447 and the γ-ray silent J1548+3511. The results for these two sources are then compared to what has been found for the other γ-ray emitting RL-NLSy1 in the literature, in order to investigate the peculiarity of this subclass of objects. The information from the multiwavelength data of J1548+3511 and PKS 2004−447 is then used to model the spectral energy distribution (SED) of these two sources.

The paper is organized as follows. In Sections 2, 3, 4, and 5 we report the radio, γ-ray *Fermi*-LAT, X-ray *Swift*, and *XMM–Newton* data analysis. In Section 6 we present the results from the multiwavelength analysis. The discussion and the presentation of the SED modelling are given in Section 7, while a brief summary is in Section 8.

Throughout this paper, we assume the following cosmology: $H_0 = 71$ km s^{-1} Mpc^{-1}, $\Omega_{\rm M} = 0.27$, and $\Omega_\Lambda = 0.73$, in a flat Universe.

2 RADIO DATA

2.1 VLBA observations

Multifrequency Very Long Baseline Array (VLBA) observation (project code BO045) of J1548+3511 was carried out at 5, 8.4, and 15 GHz on 2013 January 2. The observation was performed in phase reference mode with a recording bandwidth of 16 MHz per channel in dual polarization at 512 Mbps data rate. The target source was observed for 45 min at 5 and 8.4 GHz, and for 75 min at 15 GHz, spread into several scans and cycling through frequencies and calibrators in order to improve the *uv* coverage. The strong source 3C 345 was used as fringe finder and bandpass calibrator. The source J1602+3326 was used as phase calibrator.

Data reduction was performed using the National Radio Astronomy Observatory (NRAO)'s Astronomical Image Processing System (AIPS). A priori amplitude calibration was derived using measurements of the system temperature and the antenna gains. The uncertainties on the amplitude calibration ($\sigma_{\rm c}$) were found to be approximately 5 per cent at 5 and 8.4 GHz, and about 7 per cent at 15 GHz. Final images were produced after a number of phase self-calibration iterations (Fig. 1). The 1σ noise (rms) level measured on the image plane is about 0.08 mJy beam^{-1} at 5 and 8.4 GHz, and about 0.12 mJy beam^{-1} at 15 GHz. The restoring beam is 3.4 $\times$ 1.3, 2.1 $\times$ 0.8, and 1.1 $\times$ 0.4 mas^2 at 5, 8.4, and 15 GHz, respectively. In addition to the full-resolution images, at 5 and 8.4 GHz we produced 'low-resolution' images using natural grid weighting

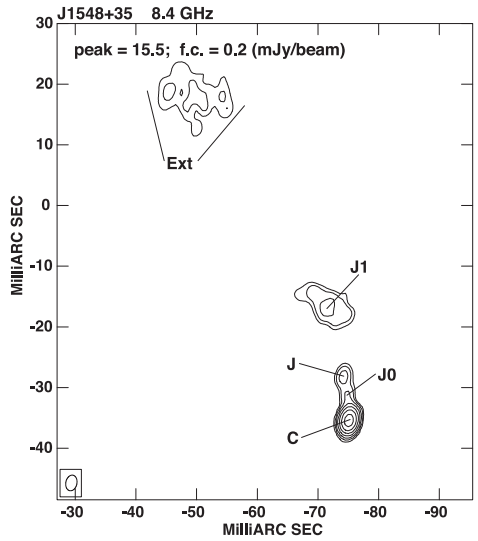

Figure 2. Low-resolution VLBA image of J1548+3511 at 8.4 GHz. On the image we provide the peak flux density in mJy beam^{-1} and the first contour intensity (f.c.) in mJy beam^{-1}, which corresponds to two times the off-source noise level measured on the image plane. Contours increase by a factor of 2. The restoring beam is plotted in the bottom left-hand corner.

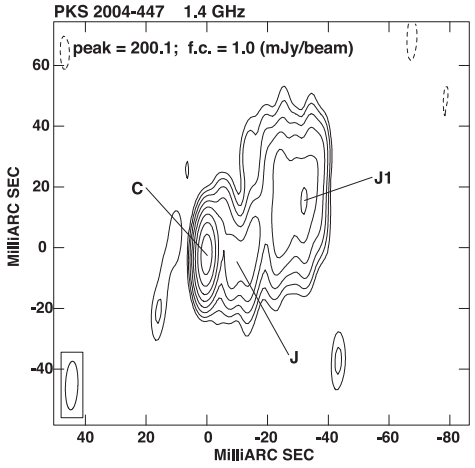

Figure 3. VLBA image at 1.4 GHz of PKS 2004−447. On the image we provide the peak flux density in mJy beam^{-1} and the first contour intensity (f.c.) in mJy beam^{-1}, which corresponds to three times the off-source noise level measured on the image plane. Contours increase by a factor of 2. The restoring beam is plotted in the bottom left-hand corner.

and a maximum baseline of 100 Mλ. The low-resolution image at 8.4 GHz is presented in Fig. 2. The restoring beam is 2.6×1.8 mas^2.

To study the parsec-scale structure of PKS 2004−447 we retrieved archival VLBA data at 1.4 GHz (project code BD050). The observation was performed on 1998 October 13 with a recording bandwidth of 8 MHz per channel in dual polarization at 256 Mbps data rate. In this observing run PKS 2004−447 was observed as phase calibrator, for a total time of about 30 min. Seven VLBA antennas participated in the observing run. Because of the southern declination of the source the restoring beam is highly elongated in the north–south direction and is 16.0×4.1 mas^2.

The data were reduced following the same procedure described for J1548+3511. The uncertainties on the amplitude calibration are $\sigma_c \sim 10$ per cent. Final images were produced after a number of phase self-calibration iterations. Amplitude self-calibration was applied using a solution interval longer than the scan length to remove residual systematic errors at the end of the self-calibration process. The final image is presented in Fig. 3. The 1σ noise level measured on the image plane is ∼0.3 mJy beam^{-1}.

The total flux density of each source was measured by using the AIPS verb TVSTAT, which performs an aperture integration over a selected region on the image plane. In the case of bright and compact components, like the core, we used the task JMFIT, which performs a Gaussian fit to the source component on the image plane. For more extended subcomponents, like jets, the flux density was measured by TVSTAT. The uncertainty in the flux density arises from both the calibration error σ_c and the measurement error σ_m. The latter represents the off-source rms noise level measured on the image plane and is related to the source size θ_{obs} normalized by the beam size θ_{beam} as $\sigma_m = \mathrm{rms}\,(\theta_{obs}/\theta_{beam})^{1/2}$. The flux density error σ_S reported in Table 1 takes both uncertainties into account and corresponds to $\sigma_S = \sqrt{\sigma_c^2 + \sigma_m^2}$.

2.2 Archival VLA data

To investigate possible flux density variability we retrieved Very Large Array (VLA) archival data for both J1548+3511 and PKS 2004−447 (see Table 2). Data were reduced following the standard procedure implemented in the AIPS package. Primary calibrators are 3C 286 and 3C 48 and the uncertainties on the amplitude calibration are between 3 and 5 per cent. VLA images were obtained after a few phase-only self-calibration iterations. Both sources are unresolved on arcsecond scale.

The errors on the VLA flux densities are dominated by the uncertainties on the amplitude calibration, being $\sigma_m \sim 0.1$ mJy beam^{-1}.

Table 1. VLBA flux density of J1548+3511 and PKS 2004−447. Column 1: source name; column 2: source component; columns 3, 4, 5, and 6: flux density at 1.4, 5, 8.4, and 15 GHz, respectively.

Freq. (GHz)	Comp.	$S_{1.4}$ (mJy)	S_5 (mJy)	$S_{8.4}$ (mJy)	S_{15} (mJy)
J1548+3511	C	–	12.9 ± 0.6	16.0 ± 0.8	20.8 ± 1.5
	J	–	3.8 ± 0.2	0.8 ± 0.1	–
	J0	–	–	1.5 ± 0.1	–
	J1	–	9.7 ± 0.6	5.1 ± 0.3	–
	Ext	–	11.0 ± 0.8	4.4 ± 0.5	–
	Tot	–	37.4 ± 2.0	27.8 ± 1.4	20.8 ± 1.5
PKS 2004−447	C	224 ± 22	–	–	–
	J	100 ± 10	–	–	–
	J1	210 ± 21	–	–	–
	Tot	534 ± 53	–	–	–

3 *FERMI*-LAT DATA: SELECTION AND ANALYSIS

The LAT on-board the *Fermi* satellite is a γ-ray telescope operating from 20 MeV to >300 GeV, with a large peak effective area (∼8000 cm^2 for 1 GeV photons), an energy resolution typically ∼10 per cent, and a field of view of about 2.4 sr with single-photon angular resolution (68 per cent containment radius) of 0.°6 at $E =$ 1 GeV on-axis. Details about the LAT are given by Atwood et al. (2009).

The LAT data reported in this paper for PKS 2004−447 and J1548+3511 were collected over the first 6 yr of *Fermi* operation, from 2008 August 4 (MJD 54682) to 2014 August 4 (MJD 56873).

Table 2. Archival VLA data. Column 1: source name; column 2: observing frequency; columns 3 and 4: date and project code of the observation; column 5: beam size; column 6: observing time; column 7: flux density.

Source	Freq (GHz)	Date	Code	Beam (arcsec^2)	Obs. time (min)	Flux (mJy)
J1548+3511	1.4	1999-04-13	AL485	49.31 × 46.17	1	136 ± 4
	1.4	2003-09-05	AL595	1.46 × 1.17	1.2	124 ± 6
	4.8	1994-05-07	AK360	0.74 × 0.39	1.0	74 ± 2
	8.4	1995-08-14	AM484	0.24 × 0.22	0.6	76 ± 2
	8.4	1999-04-13	AL485	8.46 × 7.65	0.8	54 ± 2
PKS 2004−447	8.4	1988-12-23	AP001	1.29 × 0.19	1	330 ± 17
	8.4	1995-07-15	AK394	1.15 × 0.19	4.5	270 ± 11
	8.4	2005-03-16	AK583	4.63 × 0.56	3	219 ± 11
	8.4	2005-04-21	AK583	3.65 × 0.60	6	440 ± 18

During this time, the *Fermi* observatory operated almost entirely in survey mode. The analysis was performed with the ScienceTools software package version v9r33p0.[2] Only events belonging to the 'source' class were used. The time intervals when the rocking angle of the LAT was greater than 52° were rejected. In addition, a cut on the zenith angle (<100°) was applied to reduce contamination from the Earth limb γ-rays, which are produced by cosmic rays interacting with the upper atmosphere. The spectral analysis was performed with the instrument response functions P7REP_SOURCE_V15 using an unbinned maximum likelihood method implemented in the tool GTLIKE. Isotropic ('ISO_SOURCE_V05.TXT') and Galactic diffuse emission ('GLL_IEM_V05_REV1.FIT') components were used to model the background.[3] The normalizations of both components were allowed to vary freely during the spectral fitting.

We analysed a region of interest of 10° radius centred at the location of our two targets. We evaluated the significance of the γ-ray signal from the source by means of the maximum-likelihood test statistic TS = $2(\log L_1 - \log L_0)$, where L is the likelihood of the data given the model with (L_1) or without (L_0) a point source at the position of our target (e.g. Mattox et al. 1996). The source model used in GTLIKE includes all the point sources from the third *Fermi*-LAT catalogue (3FGL; Acero et al. 2015) that fall within 15° of the target. The spectra of these sources were parametrized by power law, log-parabola, or exponential cut-off power-law model, as in the 3FGL catalogue.

A first maximum-likelihood analysis was performed to remove from the model the sources having TS < 10 and/or a predicted number of counts based on the fitted model $N_{\rm pred} < 1$. A second maximum-likelihood analysis was performed on the updated source model. In the fitting procedure, the normalization factors and the photon indices of the sources lying within 10° of the target were left as free parameters. For the sources located between 10° and 15° from the target, we kept the normalization and the photon index fixed to the values from the 3FGL catalogue.

For PKS 2004−447, the fit with a power-law model to the data integrated over 72 months of *Fermi*-LAT operation in the 0.1–100 GeV energy range results in TS = 164, with an average flux of $(1.59 \pm 0.16) \times 10^{-8}$ photons cm^{-2} s^{-1}, and a photon index $\Gamma_\gamma = 2.39 \pm 0.06$, corresponding to an energy flux of $(1.09 \pm 0.11) \times 10^{-12}$ erg cm^{-2} s^{-1}. Fig. 4 shows the γ-ray light curve of PKS 2004−447 for the period 2008 August 4–2014 August 4 using 3-month time bins. For each time bin, the photon index was frozen to the value resulting from the likelihood analysis over the whole period. The systematic uncertainty in the effective area (Ackermann et al. 2012) amounts to 10 per cent below 100 MeV, decreasing linearly with the logarithm of energy to 5 per cent between 316 MeV and 10 GeV, and increasing linearly with the logarithm of energy up to 15 per cent at 1 TeV.[4] Statistical errors dominate over the systematics uncertainty. All errors relative to γ-ray data reported throughout the paper are statistical only.

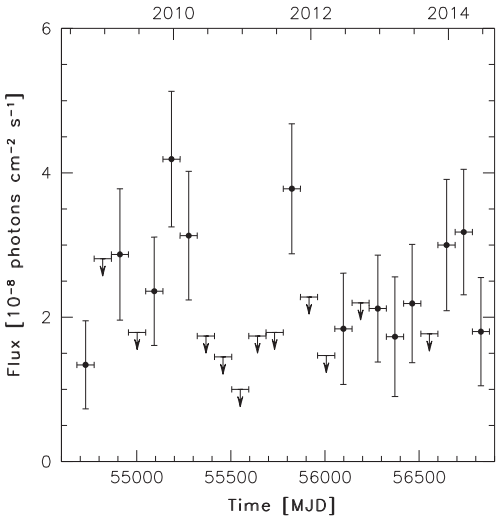

Figure 4. LAT light curve of PKS 2004−447 in the 0.1–100 GeV energy range obtained from 2008 August 4 to 2014 August 4 (MJD 54682–56873) with 3-month time bins. Downward arrows represent 2σ upper limits.

For J1548+3511, the fit with a power-law model over 6 yr of *Fermi*-LAT operation results in TS = 1. The 2σ upper limit is 3.35×10^{-8} photons cm^{-2} s^{-1} in the 0.1–100 GeV energy range (assuming a photon index $\Gamma_\gamma = 2.4$), corresponding to an energy flux $<5.3 \times 10^{-11}$ erg cm^{-2} s^{-1}.

4 *SWIFT* DATA: OBSERVATIONS AND ANALYSIS

The *Swift* satellite (Gehrels et al. 2004) performed 27 observations of PKS 2004−447 between 2011 May 15 and 2014 March 16. J1548+3511 has not been observed by *Swift* so far.

[2] http://fermi.gsfc.nasa.gov/ssc/data/analysis/software/
[3] http://fermi.gsfc.nasa.gov/ssc/data/access/lat/BackgroundModels.html
[4] http://fermi.gsfc.nasa.gov/ssc/data/analysis/LAT_caveats.html

Table 3. Log and fitting results of *Swift*-XRT observations of PKS 2004−447 using a power-law model with an H I column density fixed to the Galactic value in the direction of the source.

Date (MJD)	Date (UT)	Net exposure time (s)	Photon index Γ_X	Flux 0.3–10 keV[a] (10^{-13} erg cm^{-2} s^{-1})
55686	2011-05-05	6778	1.65 ± 0.25	5.6 ± 0.9
55756/55761/55765	2011-07-14/19/23	7101	1.62 ± 0.29	5.5 ± 0.7
55783/55786	2011-08-10/13	2258	1.15 ± 0.49	6.4 ± 2.1
55809/55821	2011-09-05/17	8239	1.38 ± 0.19	11.8 ± 1.3
55880	2011-11-15	7095	2.02 ± 0.30	4.4 ± 0.7
56000	2012-03-14	7306	1.52 ± 0.30	4.5 ± 0.8
56111/56120	2012-07-3/12	7120	1.65 ± 0.24	6.5 ± 0.9
56182/56192/56200	2012-09-12/22/30	17 016	1.63 ± 0.18	5.9 ± 0.6
56480/56487	2013-07-07/14	22 963	1.42 ± 0.12	10.4 ± 0.7
56562	2013-09-27	8361	1.45 ± 0.20	14.6 ± 1.5
56578/56585/56592/56594	2013-10-13/20/27/29	12 699	1.41 ± 0.24	8.7 ± 1.2
56599/56618	2013-11-03/19	8241	1.58 ± 0.18	6.8 ± 0.6
56619	2013-11-20	12 179	1.43 ± 0.16	15.5 ± 1.2
56730	2014-03-14	7507	1.68 ± 0.26	6.7 ± 1.0
56732	2014-03-16	9642	1.48 ± 0.19	9.0 ± 1.0

Note. [a]Unabsorbed flux.

The observations of PKS 2004−447 were carried out with all three instruments on-board: the X-Ray Telescope (XRT; Burrows et al. 2005, 0.2–10.0 keV), the Ultraviolet/Optical Telescope (UVOT; Roming et al. 2005, 170–600 nm), and the Burst Alert Telescope (BAT; Barthelmy et al. 2005, 15–150 keV). The source was not present in the *Swift* BAT 70-month hard X-ray catalogue (Baumgartner et al. 2013).

The XRT data of PKS 2004−447 were processed with standard procedures (XRTPIPELINE v0.13.0), filtering, and screening criteria using the HEASOFT package (v6.15). The data were collected in photon counting mode for all the observations. The source count rate was low (<0.5 counts s^{-1}); thus pile-up correction was not required. Source events were extracted from a circular region with a radius of 20 pixels (1 pixel = 2.36 arcsec), while background events were extracted from a circular region with radius of 50 pixels away from the source region and from other bright sources. Ancillary response files were generated with XRTMKARF, and account for different extraction regions, vignetting and point spread function corrections. We used the spectral redistribution matrices in the calibration data base maintained by High Energy Astrophysics Science Archive Research Center (HEASARC).[5] Short observations performed during the same month were summed in order to have enough statistics to obtain a good spectral fit. The spectra with low numbers of photons collected (<200 counts) were rebinned with a minimum of 1 count per bin and the Cash statistic (Cash 1979) was used. We fitted the spectra with an absorbed power law using the photoelectric absorption model TBABS (Wilms, Allen & McCray 2000), with a neutral hydrogen column density fixed to its Galactic value (3.17×10^{20} cm^{-2}; Kalberla et al. 2005). The fit results are reported in Table 3.

UVOT data of PKS 2004−447 in the v, b, u, $w1$, $m2$, and $w2$ filters were reduced with the task UVOTSOURCE included in the HEASOFT package v6.15 and the version 20130118 CALDB-UVOTA release. We extracted the source counts from a circle with 5 arcsec radius centred on the source and the background counts from a circle with 10 arcsec radius in a nearby empty region. The observed magnitudes are reported in Table 4. We converted the magnitudes into de-reddened flux densities by using the $E(B-V)$ value of 0.029 from Schlafly & Finkbeiner (2011), the extinction laws by Cardelli, Clayton & Mathis (1989), and the magnitude flux calibrations by Bessell, Castelli & Plez (1998) and Breeveld et al. (2011).

5 *XMM–NEWTON* DATA: OBSERVATIONS AND ANALYSIS

5.1 EPIC observations and data reduction

J1548+3511 was observed by *XMM–Newton* (Jansen et al. 2001) on 2011 August 8 and 20 for a total observing time of 28 ks in both cases (observation IDs 0674320301 and 0674320401). For this analysis we focus on the data from the European Photon Imaging Camera (EPIC)-pn, which was operated in the full window mode, with net exposure times of 19.4 and 22.9 ks for the two observations.

XMM–Newton observed PKS 2004−447 on 2012 May 1 and 2012 October 18 for a total duration of 36 ks in both cases (observation IDs 0694530101 and 0694530201). The EPIC-pn and the EPIC-Metal Oxide Semi-conductor (MOS) cameras (MOS1 and MOS2) were operated in the full frame mode. The first observation has net exposure times of 18, 20, and 20 ks for the pn, MOS1, and MOS2, respectively; the second observation has net exposure times of 29, 35, and 35 ks. Differently from the first observation, in the second observation there is a significant increase of counts (∼70 per cent) adding the data collected by MOS1 and MOS2 to the pn data. Therefore, for the first observation of PKS 2004−447 we focus on the data from the EPIC-pn only, while for the second observation both the pn and MOS data were analysed.

The data were reduced using the *XMM–Newton* Science Analysis System (SAS v13.5.0), applying standard event selection and filtering.[6] Neither observation was affected by background flaring. The source spectra were extracted from a circular region of radius 30 arcsec centred on the source, and the background from a nearby region on the same chip. To allow for χ^2 fitting the spectra were binned to contain at least 20 counts per bin. All errors are quoted

[5] http://heasarc.nasa.gov/

[6] http://xmm.esac.esa.int/external/xmm_user_support/documentation/sas_usg/USG/

Table 4. Results of the *Swift*-UVOT observations of PKS 2004−447 in magnitudes.

Date (MJD)	Date (UT)	v	b	u	$w1$	$m2$	$w2$
55686	2011-05-05	18.48 ± 0.18	20.08 ± 0.28	19.17 ± 0.19	19.77 ± 0.32	>19.86	>20.19
55756	2011-07-14	>18.98	19.69 ± 0.30	19.31 ± 0.28	19.29 ± 0.29	>19.40	>19.85
55761	2011-07-19	18.85 ± 0.35	–	>18.89	>19.35	>19.19	>19.61
55765	2011-07-23	>19.33	20.25 ± 0.36	19.25 ± 0.20	19.53 ± 0.28	>19.70	>20.01
55783	2011-08-10	–	–	–	19.41 ± 0.18	–	–
55786	2011-08-13	18.48 ± 0.28	19.56 ± 0.31	19.29 ± 0.33	19.67 ± 0.35	>19.87	20.37 ± 0.35
55809	2011-09-05	>18.24	>19.12	18.59 ± 0.32	>19.06	>18.98	19.74 ± 0.34
55821	2011-09-17	18.28 ± 0.25	18.99 ± 0.16	18.77 ± 0.18	18.84 ± 0.24	>19.30	>19.50
55880	2011-11-15	>18.61	19.63 ± 0.32	>19.25	>19.33	>19.40	>19.52
56000	2012-03-14	>18.94	>19.76	>19.41	>19.59	>19.70	19.55 ± 0.25
56111	2012-07-03	–	–	–	19.48 ± 0.11	–	–
56120	2012-07-12	–	–	–	–	19.94 ± 0.35	–
56182	2012-09-12	18.45 ± 0.24	19.67 ± 0.30	18.91 ± 0.22	19.46 ± 0.28	19.62 ± 0.14	20.00 ± 0.23
56192	2012-09-22	>18.90	19.36 ± 0.23	18.72 ± 0.19	19.37 ± 0.32	19.70 ± 0.27	20.27 ± 0.30
56200	2012-09-30	–	–	19.10 ± 0.09	–	–	–
56480	2013-07-07	–	–	18.87 ± 0.09	–	–	19.91 ± 0.20
56487	2013-07-14	–	–	18.56 ± 0.07	19.36 ± 0.10	–	–
56562	2013-09-27	–	–	–	19.03 ± 0.09	19.28 ± 0.11	–
56578	2013-10-13	–	–	–	–	19.81 ± 0.23	–
56585	2013-10-20	–	–	–	–	–	19.77 ± 0.15
56592	2013-10-27	–	–	18.69 ± 0.21	–	–	19.54 ± 0.25
56594	2013-10-29	–	–	–	–	19.91 ± 0.23	–
56599	2013-11-03	–	–	–	19.28 ± 0.27	–	–
56618	2013-11-19	–	–	–	18.85 ± 0.15	–	–
56619	2013-11-20	–	–	18.30 ± 0.06	–	–	–
56730	2014-03-14	–	–	–	19.67 ± 0.16	>19.56	–
56732	2014-03-16	–	–	18.59 ± 0.11	–	–	–

Table 5. Fits to the 0.3–10 keV EPIC-pn spectra of J1548+3511. Galactic absorption was included in all fits.

Model	Parameter	Value Obs 1	Value Obs 2
Power law	Γ	2.47 ± 0.06	2.31 ± 0.05
	Norm	$7.8 \pm 0.2 \times 10^{-5}$	$9.0 \pm 0.2 \times 10^{-5}$
	χ^2/d.o.f.	129/129	210/164
Broken power law	Γ_1	$2.57^{+0.09}_{-0.08}$	$2.49^{+0.09}_{-0.08}$
	$E_{\rm break}$ (keV)	$2.0^{+0.8}_{-0.5}$	$1.7^{+0.5}_{-0.3}$
	Γ_2	$1.9^{+0.3}_{-0.4}$	1.7 ± 0.2
	Norm	$7.5^{+0.3}_{-0.4} \times 10^{-5}$	$8.4^{+0.3}_{-0.4} \times 10^{-5}$
	χ^2/d.o.f.	110/127	154/162

at the 90 per cent confidence level for the parameter of interest (corresponding to $\Delta\chi^2 = 2.7$).

5.2 X-ray spectral analysis

5.2.1 J1548+3511

The spectral fits were performed over the 0.3–10 keV energy range using XSPEC v.12.8.1. Although we present only the fits to the EPIC-pn, the results were cross-checked for consistency with the MOS spectra. Galactic absorption of 2.19×10^{20} cm^{-2} was included in all fits using the TBABS model. In the 2 weeks between the observations the unabsorbed flux increased from $F_{0.3-10\,\rm keV} = (4.2 \pm 0.2) \times 10^{-13}$ to $(5.3 \pm 0.2) \times 10^{-13}$ erg cm^{-2} s^{-1}. No strong variability was seen during the individual observations.

The results of fitting a single power law and a broken power law to the two spectra are summarized in Table 5 and shown in Fig. 5. While the single power-law model leaves positive residuals above 3 keV, the broken power law is a good fit to the data. The improvement between the models is more significant in the second observation, when the source was brighter. In this model the spectral shape changes from a soft slope of $\Gamma_1 = 2.6 \pm 0.1$ (2.5 ± 0.1) below $E_{\rm break} = 2.0^{+0.8}_{-0.5}$ keV (1.7 ± 0.2 keV) to $\Gamma_2 = 1.9^{+0.3}_{-0.4}$ ($\Gamma_2 = 1.7 \pm 0.2$) above $E_{\rm break}$ for the first (second) observation. If we add to the models another neutral absorber at the redshift of the source the fits do not improve, showing that no intrinsic absorption is required. Furthermore, there is no detection of an Fe line, with 90 per cent upper limits on a narrow line at 6.4 keV of EW < 0.26 and <0.13 keV for the first and second observation, respectively. Unfortunately, the data quality is not sufficient to obtain meaningful constraints on more complex models for the emission.

5.2.2 PKS 2004−447

As for J1548+3511, the spectral fits were performed over the 0.3–10 keV energy range using XSPEC v.12.8.1. Although for the first observation we present only the fits to the EPIC-pn, the results were cross-checked for consistency with the MOS spectra. Galactic absorption of 3.17×10^{20} cm^{-2} was included in all fits using the TBABS model. In the 5 months between the observations the unabsorbed flux increased from $F_{0.3-10\,\rm keV} = (4.5 \pm 0.1) \times 10^{-13}$ to $(6.8 \pm 0.2) \times 10^{-13}$ erg cm^{-2} s^{-1}. No strong variability was seen during the individual observations.

The results of fitting a single power law and a broken power law to the two spectra are summarized in Table 6. No significant soft X-ray excess is observed below 2 keV. A simple power-law model (Fig. 6) is sufficient to describe the data of the first observation. For the second observation the power law is not an optimal fit ($\chi^2 = 273/241$, Table 6), but no significant improvement was obtained using a broken power-law model. We note a dip in the residuals of the

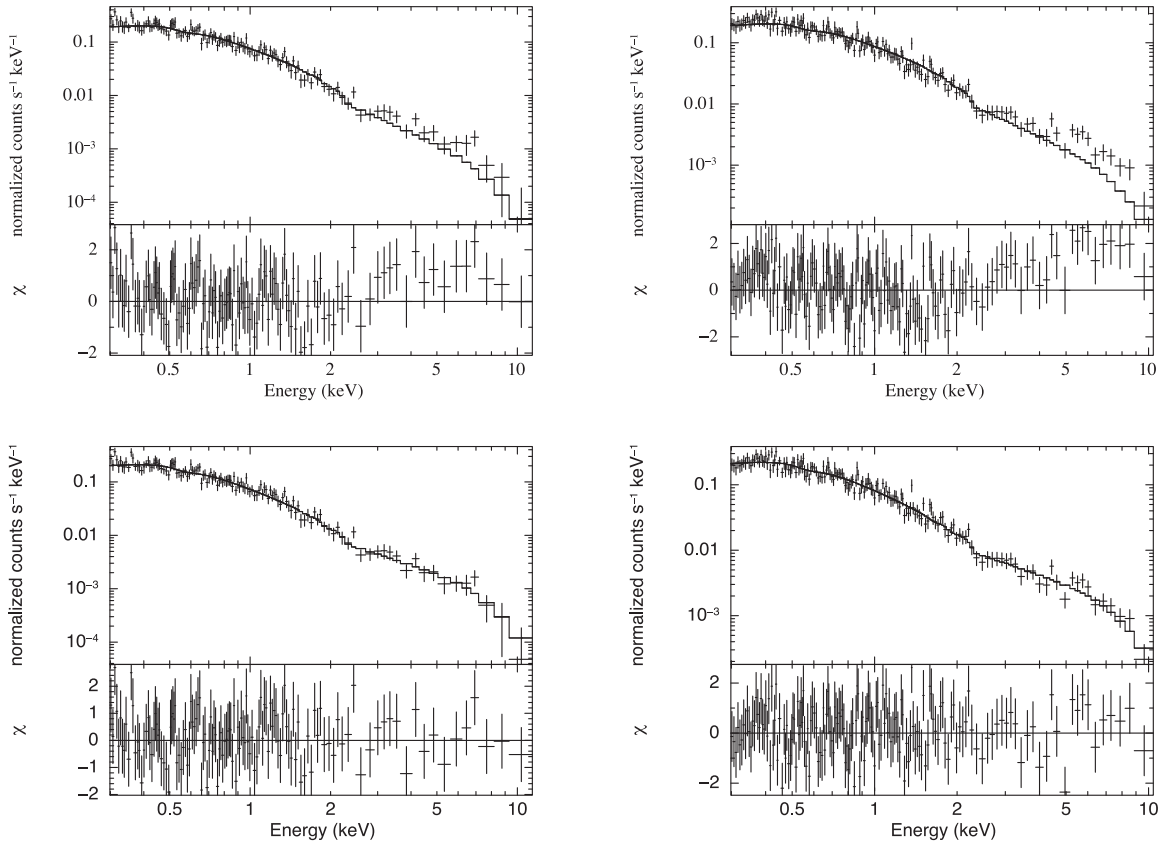

Figure 5. EPIC-pn spectra and residuals of J1548+3511 fitted with a power law (upper panel) and a broken power law (lower panel). The first observation is shown to the left and the second one to the right.

second observation at ∼0.7 keV. Adding to the model an absorption edge, the fit is slightly better ($\chi^2 = 263/239$) with a threshold energy $E_c = 0.77^{+0.05}_{-0.11}$ keV, compatible with the O VII absorption, and a maximum optical depth $\tau = 0.21^{+0.14}_{-0.11}$. However, observations with better statistics are required to confirm this feature.

In both observations, the photon index is $\Gamma_X \sim 1.7$, consistent with a jet emission component. Similarly to J1548+3511, if we add to the models another neutral absorber at the redshift of the source the fits do not improve, showing that no intrinsic absorption is required. Moreover, there is no detection of an Fe line, with 90 per cent upper limits on a narrow line at 6.4 keV of EW < 0.12 and <0.05 keV for the first and second observation, respectively.

5.3 Optical Monitor data

The Optical Monitor (OM; Mason et al. 2001) on-board *XMM–Newton* is a 30-cm telescope carrying six optical/UV filters and two grisms. We used the SAS task OMICHAIN to reduce the data and the tasks OMSOURCE and OMPHOTOM to derive the source magnitude.

The OM was operated during all the observations described in Section 5.1. J1548+3511 was observed twice in optical and UV bands. Average observed magnitudes for J1548+3511 are reported in Table 7. No significant change of activity was observed for J1548+3511 between the two OM observations. PKS 2004−447 was observed by OM in *u* band, with observed magnitudes $u = 19.20 \pm 0.03$ and 18.92 ± 0.03 for 2012 May 1 and 2012 October 18, respectively. Therefore, on a half-year time-scale a difference of ∼0.3 mag was observed in optical for PKS 2004−447.

6 RESULTS

6.1 The NLSy1 J1548+3511

6.1.1 Radio properties

In the radio band, the NLSy1 J1548+3511 shows a core–jet structure with a total angular size of about 70 mas corresponding to a linear size of 420 pc (Fig. 1). Component C accounts for the majority of the VLBA flux density, from about 34 per cent at 5 GHz up to 100 per cent at 15 GHz. Its inverted spectrum ($\alpha \sim -0.4$; $S_\nu \propto \nu^{-\alpha}$) indicates that is the source core. From the core region a one-sided jet emerges with a position angle of about 10° and bends to the east (position angle of about 30°) at a distance of ∼40 mas (240 pc) from the core, where the component J1 is observed. The higher resolution provided by 8.4-GHz data allows us to resolve the innermost part of the jet into two compact components (labelled J and J0 in Fig. 1), which are likely jet knots. An extended low surface brightness structure (labelled Ext in Figs 1 and 2) is observed at ∼60 mas (360 pc) from the core. At 15 GHz only the core component is detected.

The source is unresolved on the arcsecond scale sampled by VLA images. The similar flux density (∼141 mJy) reported in the NRAO VLA Sky Survey (NVSS; Condon et al. 1998) and the Faint Images of the Radio Sky at Twenty cm (FIRST; Becker, White & Helfand 1995) indicates that no extended emission on arcsecond scale is present. On the other hand, VLBA observations at 5 and 8.4 GHz could recover only about 50 per cent or less of the VLA flux density. This may be due to a combination of both variability and the presence of extended jet structure that cannot be imaged

Table 6. Fits to the 0.3–10 keV EPIC spectra of PKS 2004−447. Galactic absorption was included in all fits.

Model	Parameter	Value Obs 1	Value Obs 2
Power law	Γ	1.72 ± 0.05	1.69 ± 0.03
	Norm	$7.0 \pm 0.2 \times 10^{-5}$	$10.0 \pm 0.3 \times 10^{-5}$
	χ^2/d.o.f.	97/102	273/241
Broken power law	Γ_1	1.76 ± 0.07	1.71 ± 0.03
	$E_{\rm break}$ (keV)	$2.0^{+2.0}_{-0.9}$	$3.3^{+1.2}_{-0.6}$
	Γ_2	1.63 ± 0.19	1.51 ± 0.14
	Norm	7.0×10^{-5}	$10.4 \pm 0.3 \times 10^{-5}$
	χ^2/d.o.f.	96/100	268/239

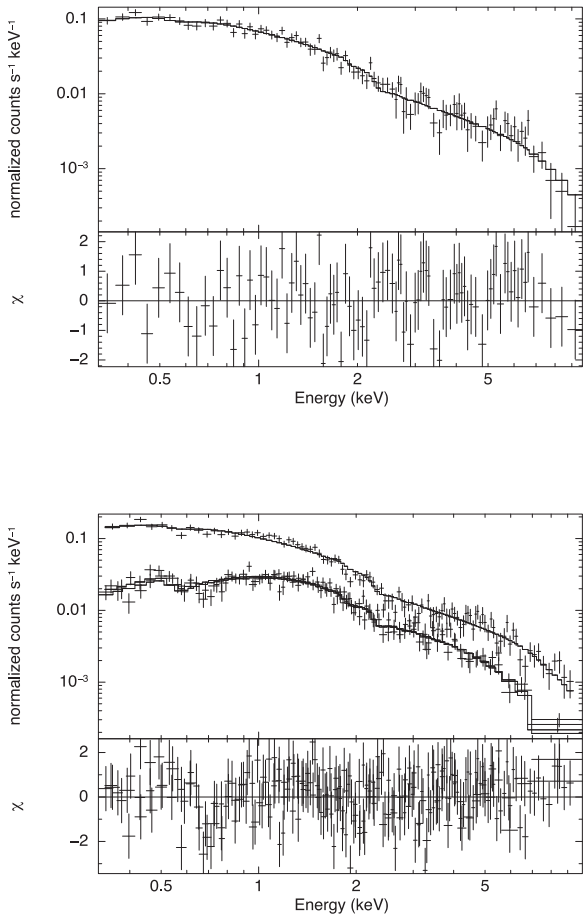

Figure 6. EPIC spectra and residuals of PKS 2004−447 fitted with a power law. For the first observation (upper panel) only EPIC-pn data were considered, while for the second (bottom panel) EPIC-pn, MOS1, and MOS2 were considered in the fit.

by the short baselines of the VLBA. The spectral index computed using VLA data between 1.4 and 8.4 GHz results in a moderately flat spectrum with $\alpha \sim 0.3$–0.4. However, the spectral index values are strongly subject to the flux density variability observed in this source.

A small part of the flux density from the extended low surface brightness structure is recovered in the low-resolution image at 8.4 GHz (Fig. 2), where the total flux density is ∼28 mJy instead of 21 mJy measured on the high-resolution image. No significant difference between the flux density measured in low- and high-resolution images is found at 15 GHz.

We investigated the source variability by the analysis of archival VLA data. Although the data sets considered are not homogeneous (i.e. different VLA configurations), the lack of extended emission on arcsecond scale implies that variation in the flux density should be intrinsic to the source and not related to the lack of short baselines in the extended VLA configurations. Evidence for intrinsic variability comes from observations at 8.4 GHz, where the highest flux density was measured when the VLA was in the most extended configuration (Table 2).

For each frequency we computed the variability index V following Hovatta et al. (2008):

$$V = \frac{(S_{\rm max} - \sigma_{\rm max}) - (S_{\rm min} + \sigma_{\rm min})}{(S_{\rm max} - \sigma_{\rm max}) + (S_{\rm min} + \sigma_{\rm min})}, \quad (1)$$

where $S_{\rm max}$ and $S_{\rm min}$ are the maximum and minimum flux density, whereas $\sigma_{\rm max}$ and $\sigma_{\rm min}$ are their associated errors, respectively.

In addition to the VLA flux density reported in Table 2, at 1.4 GHz we considered the values from the FIRST and NVSS, while at 5 GHz we considered the values reported in the 87 GB catalogue (Gregory & Condon 1991) and in the second MIT-Green Bank Survey (Langston et al. 1990). VLBA flux densities were not taken into account due to the possible missing flux from extended jet structures on parsec scales. From equation (1) we found that V is 1, 11, and 14 per cent at 1.4, 5, and 8.4 GHz, respectively, indicating larger variability at higher frequencies as usually found in blazars. The low variability ($V = 0.01$) estimated at 1.4 GHz is comparable to the uncertainties. We note that the flux density variability may be underestimated due to the poor time sampling of the observations.

6.1.2 X-ray properties

In the 2 weeks between the observations the source brightened by about 25 per cent. The *XMM–Newton* spectra of J1548+3511 are well fitted by a broken power-law model, with a possible Seyfert component below ∼2 keV and a jet component dominating at higher energies. The low-energy component, with a steep photon index of ∼2.5, may be associated with the soft X-ray excess. On the other hand, the relatively hard X-ray spectrum above the energy break ($\Gamma_2 = 1.7$–1.9) may suggest a significant contribution of inverse Compton radiation from a relativistic jet.

6.1.3 Optical and UV properties

No significant change of activity was observed for J1548+3511 in the optical and UV bands between the two *XMM*-OM observations performed 2 weeks apart (Table 7).

6.2 The NLSy1 PKS 2004−447

6.2.1 Radio properties

The radio source PKS 2004−447 has a core–jet structure with a total angular size of about 40 mas, which corresponds to ∼150 pc at the redshift of the source. The radio emission is dominated by the source core, labelled C in Fig. 3, which accounts for ∼42 per cent of the total flux density at 1.4 GHz. The jet structure emerges from the core component with a position angle of about −90°, then at 20 mas (∼75 pc) it bends to a position angle of about −60°. The jet structure is resolved into two subcomponents, J and J1, which are enshrouded by diffuse emission. The lack of multifrequency observations does not allow us to study the spectral index distribution across the source.

Table 7. Results of the *XMM*-OM observations of J1548+3511 in magnitudes.

Date (MJD)	Date (UT)	v	b	u	$w1$	$m2$	$w2$
55781	2011-08-08	18.10 ± 0.10	18.30 ± 0.03	17.37 ± 0.02	16.99 ± 0.02	16.62 ± 0.08	16.77 ± 0.07
55793	2011-08-20	17.99 ± 0.07	–	17.28 ± 0.02	16.99 ± 0.02	16.68 ± 0.08	16.78 ± 0.09

The source is unresolved in VLA images at 8.4 GHz, in agreement with previous studies at arcsecond-scale resolution by Gallo et al. (2006).

Archival VLA observations at 8.4 GHz point out some level of flux density variability (Table 2). From equation (1) we computed the variability index for PKS 2004−447, which turns out to be 27 per cent, consistent with the flux density variability derived from the Ceduna observations at 6.65 GHz (Gallo et al. 2006).

6.2.2 γ-ray properties

During the first 6 yr of *Fermi*-LAT observations, the 0.1–100 GeV averaged flux is $\sim 1.6 \times 10^{-8}$ photons cm^{-2} s^{-1}. The LAT light curve indicates variable γ-ray emission with flux ranging (1.3–4.2) $\times 10^{-8}$ photons cm^{-2} s^{-1}, interleaved by periods of low activity, when the source is not detected by *Fermi*-LAT (Fig. 4). No γ-ray flares from this source have been detected so far.

6.2.3 X-ray properties

The X-ray light curve collected by *Swift*-XRT indicates significant flux variability between 2011 and 2014, ranging (5–16) $\times$ 10^{-13} erg cm^{-2} s^{-1} (Fig. 7). In 2011 September the increase of the X-ray flux occurs when the γ-ray emission is in a maximum, suggesting a possible correlation between the emission in these two energy bands. On the other hand, between 2013 September and November the X-ray light curve shows two high-activity episodes in which the flux is $F_{0.3-10\,\mathrm{keV}} \sim 15 \times 10^{-13}$ erg cm^{-2} s^{-1}, interleaved by low-activity state. During the X-ray high-activity state in 2013 November, the γ-ray flux is roughly 2.6 times the average value, whereas in 2013 August–October the source is not detected in γ-rays. No significant X-ray photon index variability is observed (Fig. 7).

In the 5 months between the *XMM–Newton* observations the source brightened by about 35 per cent. The photon index derived for the two *XMM–Newton* observations is in good agreement with the *Swift*-XRT results, and is slightly softer than the value obtained in 2001 by Gallo et al. (2006). This may be due to the higher flux observed in 2001 ($F_{0.3-10\,\mathrm{keV}} = 1.5 \times 10^{-12}$ erg cm^{-2} s^{-1}) than that observed in the 2012 *XMM–Newton* observations. In the 2012 *XMM–Newton* observations, there is no evidence of soft X-ray excess.

6.2.4 Optical and UV properties

On monthly time-scales a difference of $\sim$0.3 mag was observed for PKS 2004−447 in u band by *XMM*-OM. During the *Swift*-UVOT observations the change of magnitudes spanned in the various band is about 0.6, 1.3, 1.0, 0.9, 0.7, 0.8 going from the v to $w2$ filter (Table 4). A first peak of the optical/UV activity was observed on 2011 September 5, during a high X-ray and γ-ray activity period. A second peak of activity was observed in the u and $w1$ bands on 2013 November 19 and 20. At that time, the maximum X-ray flux was observed together with a high γ-ray flux level. A contemporaneous increase of activity between the optical–UV and the X-ray and γ-ray bands indicates that the jet emission is dominant also in optical and UV, in agreement with the lack of a significant disc emission suggested by Abdo et al. (2009).

7 DISCUSSION

7.1 Relativistic jets in RL-NLSy1

High-energy emission has been detected in RL-NLSy1. On the other hand, no γ-ray emission has been found in RQ-NLSy1, suggesting a possible intrinsically different nature between these two subpopulations. Different γ-ray properties have been observed in the six RL-NLSy1 detected by *Fermi*-LAT. Three objects, PMN J0948+0022, SBS 0846+513, and 1H 0323+342 show γ-ray flares, reaching an intrinsic apparent luminosity as high as 10^{48} erg s^{-1} (D'Ammando et al. 2012, 2015a), i.e. comparable to those shown by flat-spectrum radio quasars (FSRQs; e.g. Ackermann et al. 2011). On the other hand, PKS 2004−447, PKS 1502+036, and FBQS J1644+2619 have not shown strong flares so far.

During the first 6 yr of *Fermi* operation, the apparent luminosity of PKS 2004−447 ranges $L_\gamma = (1.3–4.2) \times 10^{45}$ erg s^{-1}. A similar behaviour was found for PKS 1502+036 with a slightly larger luminosity ($L_\gamma \sim 10^{46}$ erg s^{-1}; D'Ammando et al. 2013a). FBQS J1644+2619 had an intermediate behaviour with high activity episodes interleaved by long quiescent periods (D'Ammando et al. 2015b).

The RL-NLSy1 J1548+3511 is not detected in γ-rays and the upper limit to the apparent isotropic luminosity is $L_\gamma < 1.7 \times 10^{46}$ erg s^{-1}.

The detection of γ-ray emission in a handful of RL-NLSy1 proves the presence of relativistic jets in this peculiar subclass of active galactic nuclei (AGN). In the photon index versus γ-ray luminosity plane, the γ-ray loud NLSy1 are located in the low-luminosity tail of FSRQ distribution, where also the γ-ray emitting steep-spectrum radio quasars are found (Abdo et al. 2010a; Ackermann et al. 2015).

A jet component contribution is likely observed above 2 keV in the RL-NLSy1 J1548+3511, where the X-ray photon index is $\Gamma_X \sim 1.7–1.9$. Below 2 keV the spectrum is softer, compatible with the presence of soft X-ray excess usually observed in NLSy1 (Grupe et al. 2010), as well as in the γ-ray NLSy1 PMN J0948+0022 (D'Ammando et al. 2014) and 1H 0323+342 (Paliya et al. 2014). An indication of a weak soft excess was reported by Gallo et al. (2006) for PKS 2004−447 in 2004. The X-ray spectra of PKS 2004−447 observed in 2012 are well reproduced by a single power law with hard photon index $\Gamma_X \sim 1.7$ and no significant soft X-ray excess is needed below 2 keV. This may be due to the relatively low statistics of the 2012 observations. The study of the multiwavelength variability of PKS 2004−447 indicates that during the high activity state observed in γ-rays between 2011 August and October, when the γ-ray flux was a factor of 2.6 times the average value, also the X-ray, UV, and optical emission reached a maximum, suggesting a common origin for the multiband variability. It is worth mentioning that not all the episodes of flux increase in X-rays/UV are associated with a high activity state in γ-rays (Fig. 7), like in the case of the

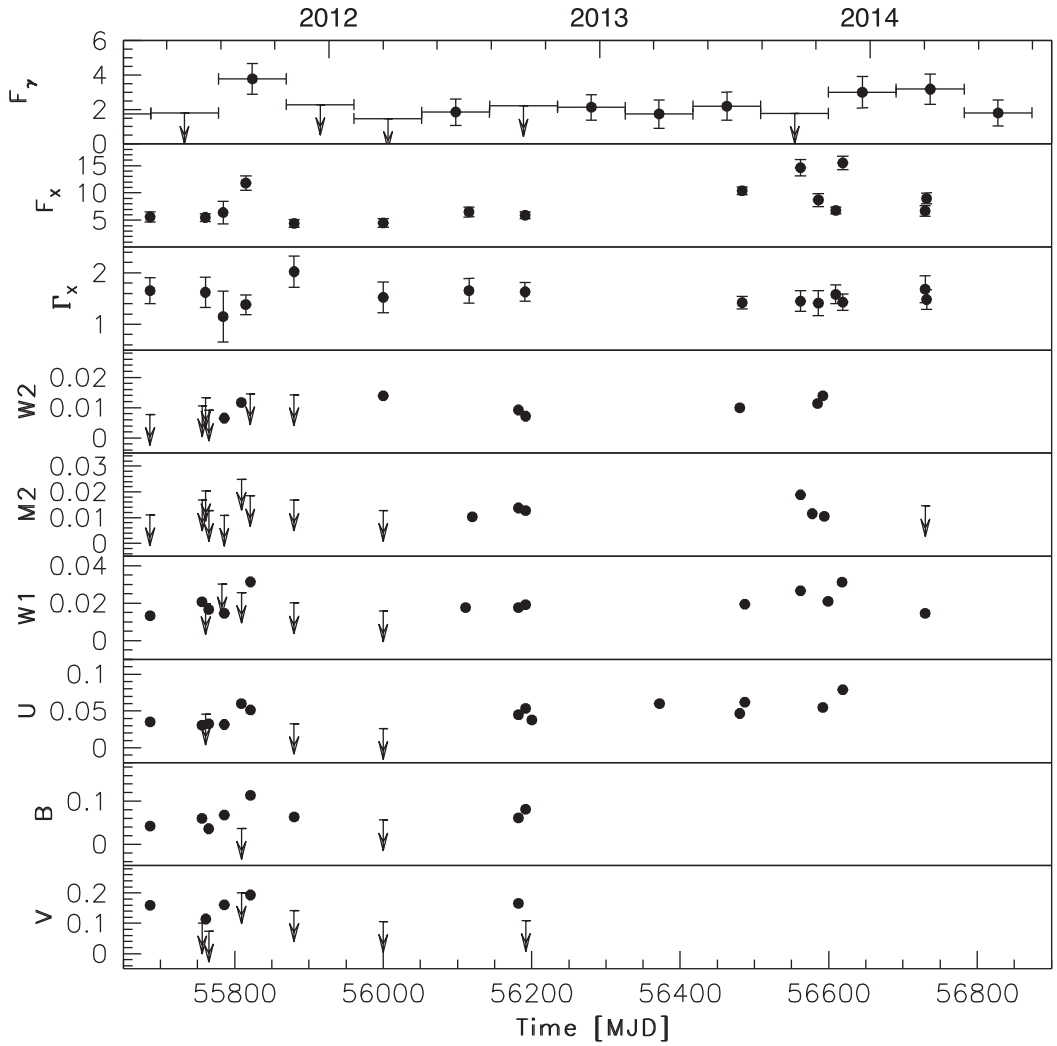

Figure 7. Multifrequency light curve of PKS 2004−447 for the period between 2011 May and 2014 August. The LAT γ-ray light curve (in units of 10^{-8} photons cm^{-2} s^{-1} for $0.1 < E < 100$ GeV; upper panel), the *Swift* X-ray light curve (in units of 10^{-13} erg cm^{-2} s^{-1} for $0.3 < E < 10$ keV; second panel from top), the X-ray photon index trend (third panel), the *Swift*-UVOT light curve in the optical and UV filters (v, b, u, $w1$, $m2$, $w2$, in units of mJy; fourth to ninth panel). Arrows refer to 2σ and 3σ upper limits on the source flux for LAT and *Swift*-UVOT measurements, respectively.

high X-ray activity observed in 2013 September. Such X-ray/UV flares with no obvious counterpart in other bands were observed in the RL-NLSy1 PMN J0948+0022 (e.g. Foschini et al. 2012), as well as in many blazars (e.g. 3C 279; Abdo et al. 2010b).

No systematic studies of complete samples of NLSy1 have been carried out at very high energy (VHE) so far. PKS 2004−447 was observed by the High Energy Stereoscopic System (H.E.S.S.; Aharonian et al. 2006). No detection was obtained and the estimated upper limit was 0.9 per cent of the Crab units (Abramowski et al. 2014). Upper limits of 10 and 1.9 per cent of the Crab units at VHE were obtained for the NLSy1 1H 0323+342 (Falcone et al. 2004) and PMN J0948+0022 (D'Ammando et al. 2015a), respectively. The lack of VHE detection may be due either to an intrinsically soft γ-ray spectrum, or to γ–γ absorption within the source, or to pair production from γ-ray photons of the source and the infrared (IR) photons from the extragalactic background light (EBL), although the latter scenario is disfavoured by the fact that the redshift of the most distant FSRQ detected at VHE, PKS 1441+25 (Mirzoyan 2015; Mukherjee 2015), is higher ($z = 0.939$) than the redshifts of the RL-NLSy1 investigated so far.

7.2 Physical properties

Milliarcsecond resolution observations are a fundamental requirement for describing the morphology and understanding the physical properties of RL-NLSy1. Given their compactness on arcsecond scale, the high angular resolution provided by VLBA observations allows us to investigate the presence of a jet structure emerging from the core region and to constrain the physical characteristics of the core emission without substantial contamination from the jet.

We computed the brightness temperature T_B of the core component by using

$$T_B = \frac{1}{2k}\frac{S(\nu)}{\Omega}\left(\frac{c}{\nu}\right)^2, \quad (2)$$

where k is the Boltzmann constant, Ω is the solid angle of the emitting regions, $S(\nu)$ is the source-frame flux density at the observed frequency, and c is the speed of light. We computed the source-frame flux density as $S(\nu) = S_{obs}(\nu)(1+z)^{1-\alpha}$, where $S_{obs}(\nu)$ is the observer-frame flux density, z is the source redshift, and α is

the radio spectral index that we assume to be equal to 0 for the self-absorbed core component. The solid angle is given by

$$\Omega = \frac{\pi}{4}\theta_{\rm min}\theta_{\rm maj}, \quad (3)$$

where $\theta_{\rm maj}$ and $\theta_{\rm min}$ are the major axis and minor axis, respectively. In both sources the core region is unresolved by our VLBA observations and the major and minor axes must be considered as upper limits. This ends up in a lower limit to the brightness temperature.

If in equation (2) we consider the values derived from the VLBA image at 15 GHz, we obtain a brightness temperature $T_{\rm B} > 4.4 \times 10^9$ K for J1548+3511. In the case of PKS 2004−447 we computed the core brightness temperature making use of the values derived from the VLBA image at 1.4 GHz, and we obtained $T_{\rm B} > 2 \times 10^{10}$ K.

For PKS 2004−447, the availability of two VLA observations separated by about 1 month allowed us to estimate the rest-frame variability brightness temperature, $T'_{\rm B,var}$, by using the flux density variability. Following D'Ammando et al. (2013a) we computed $T'_{\rm B}$ by

$$T'_{\rm B,var} = \frac{2}{\pi k}\frac{|\Delta S| D_L^2}{\Delta t^2 \nu^2 (1+z)^{1+\alpha}}, \quad (4)$$

where $|\Delta S|$ is the flux density variation, Δt is the time lag between the observations, and D_L is the luminosity distance. If in equation (4) we consider $|\Delta S| = 221$ mJy and $\Delta t = 36$ d, i.e. the flux density variation measured between the last two VLA observations, we obtain $T'_{\rm B,var} \sim 1.7 \times 10^{14}$ K. This high variability brightness temperature is similar to the value derived by Gallo et al. (2006) on the basis of Ceduna monitoring campaign. In the case of J1548+3511, Yuan et al. (2008) estimated a variability brightness temperature $T'_{\rm B,var} = 10^{13}$ K on the basis of the flux density variation measured in 207 d at 4.9 GHz. Assuming that such high values are due to Doppler boosting, we can estimate the variability Doppler factor, $\delta_{\rm var}$, by using

$$\delta_{\rm var} = \left(\frac{T'_{\rm B,var}}{T_{\rm int}}\right)^{\frac{1}{3+\alpha}}, \quad (5)$$

where $T_{\rm int}$ is the intrinsic brightness temperature. Assuming a typical value $T_{\rm int} = 5 \times 10^{10}$ K, as derived by e.g. Readhead (1994) and Hovatta et al. (2009), and a flat spectrum with $\alpha = 0$, we obtain $\delta = 15$ and 5.8 for PKS 2004−447 and J1548+3511, respectively. These values are in agreement with the range of variability Doppler factor found for the RL-NLSy1 SBS 0846+513 (D'Ammando et al. 2013b), PKS 1502+036 (D'Ammando et al. 2013a), as well as for blazars (Savolainen et al. 2010).

We estimated the ranges of viewing angles θ and of the bulk velocity in terms of speed of light β from the jet/counter-jet brightness ratio. Assuming that the source has two symmetrical jets of the same intrinsic power, we used the equation

$$\frac{B_{\rm j}}{B_{\rm cj}} = \left(\frac{1+\beta\cos\theta}{1-\beta\cos\theta}\right)^{2+\alpha}, \quad (6)$$

where $B_{\rm j}$ and $B_{\rm cj}$ are the jet and counter-jet brightness, respectively. We prefer to compare the surface brightness instead of the flux density because the jet has a smooth structure without clear knots. The jet brightness for J1548+3511 and PKS 2004−447 is 0.93 and 14.0 mJy beam^{-1}, respectively. In the case of the counter-jet, which is not visible, we assumed an upper limit for the surface brightness that corresponds to 0.2 and 0.6 mJy beam^{-1} for J1548+3511 and PKS 2004−447, respectively, i.e. 1σ noise level measured on the image. From the brightness ratio estimated from equation (6) we obtain $\beta\cos\theta > 0.61$ for J1548+3511 and >0.52 for PKS 2004−447, implying that the minimum velocity is $\beta > 0.6$ and >0.5 and a maximum viewing angle $\theta = 52^\circ$ and 59°, respectively. These limits do not provide a tight constraint on the physical parameters of these objects.

7.3 SED modelling

We created an average SED for the two NLSy1 studied here. The SED of PKS 2004−447 includes the 6-yr average *Fermi*-LAT spectrum, the *XMM–Newton* EPIC-pn data collected on 2012 October 18, and the *Swift*-UVOT data collected on 2012 September 12. In addition, we included the IR data collected by *Wide-field Infrared Survey Explorer* (*WISE*) on 2010 April 14 and by Siding Spring Observatory in 2004 April 10–12, the radio VLA and VLBA data presented in this paper, and the Australia Telescope Compact Array (ATCA) data from Gallo et al. (2006). The SED of J1548+3511 includes the upper limit estimated over 6 yr of *Fermi* observations, the *XMM–Newton* (EPIC-pn and OM) data collected on 2011 August 8, the IR data collected by *WISE* on 2010 January 30 and by Two Micron All Sky Survey (2MASS) on 1998 April 3, and the radio VLA data presented here. The multiwavelength data are not simultaneous.

We modelled the two SED with a combination of synchrotron, synchrotron self-Compton (SSC), and external Compton (EC) non-thermal emission. The synchrotron component considered is self-absorbed below 10^{11} Hz and thus cannot reproduce the radio emission. This emission is likely from the superposition of multiple self-absorbed jet components (Königl 1981). We also included thermal emission by an accretion disc and dust torus. The modelling details can be found in Finke, Dermer & Böttcher (2008) and Dermer et al. (2009). Additionally, a soft excess was observed in the X-ray spectrum of J1548+3511. We note that the origin of this soft X-ray emission is uncertain. In order to account for this feature, as a possible origin, we included emission from the disc, which is Compton scattered by an optically thin thermal plasma near the accretion disc (i.e. a corona). This was done using the routine 'SIMPL' (Steiner et al. 2009). This routine has two free parameters: the fraction of disc photons scattered by the corona ($f_{\rm sc}$), and the power-law photon index of the scattered coronal emission ($\Gamma_{\rm sc}$). The mass of the BH was chosen to be the same as the one reported in Foschini et al. (2015).

The results of the modelling are reported in Table 8 and Fig. 8 (for a description of the model parameters see Dermer et al. 2009). This model assumes that the emitting region is outside the broad-line region, where dust torus photons are likely the seed photon source. This seed photon source was modelled as being an isotropic, monochromatic radiation source with dust parameters chosen to be consistent with the relation between inner radius, disc luminosity, and dust temperature from Nenkova et al. (2008).

The Compton component of the SED of PKS 2004−447 and J1548+3511 is modelled with an external Compton scattering of dust torus seed photons, as for the SED of SBS 0846+513 (D'Ammando et al. 2013b) and PMN J0948+0022 (D'Ammando et al. 2015a). In PKS 2004−447 the IR data are not well fitted by the model. This may be due to the fact that the data considered in the SED are not simultaneous and some variability may be present (note that these data are not well fitted by the modelling done by Paliya et al. 2013 either). We note that the disc luminosity of PKS 2004−447 is particularly weak. This value is similar to the disc luminosity of SBS 0846+513, while it is significantly lower than that of PMN J0948+0022. The disc luminosity of PKS 2004−447

Table 8. Parameters used to model the SED.

Parameter	Symbol	PKS 2004−447	J1548+3511
Redshift	z	0.24	0.478
Bulk Lorentz factor	Γ	30	30
Doppler factor	$\delta_{\rm D}$	30	30
Magnetic field (G)	B	0.5	2.0
Variability time-scale (s)	$t_{\rm v}$	10^5	10^5
Comoving radius of blob (cm)	$R'_{\rm b}$	7.3×10^{16}	6.1×10^{16}
Low-energy electron spectral index	p_1	2.5	2.5
High-energy electron spectral index	p_2	3.8	3.6
Minimum electron Lorentz factor	$\gamma'_{\rm min}$	1.0	3.0
Break electron Lorentz factor	$\gamma'_{\rm brk}$	6.0×10^2	1.0×10^2
Maximum electron Lorentz factor	$\gamma'_{\rm max}$	4.0×10^3	1.0×10^4
Black hole mass ($M_\odot$)	$M_{\rm BH}$	4.3×10^6	8.3×10^7
Disc luminosity (erg s^{-1})	$L_{\rm disc}$	1.8×10^{42}	1.4×10^{45}
Inner disc radius ($R_{\rm g}$)	$R_{\rm in}$	6.0	2.0
Outer disc radius ($R_{\rm g}$)	$R_{\rm out}$	200	200
Fraction of disc photons scattered by corona	$f_{\rm sc}$	0	0.08
Corona spectral index	$\Gamma_{\rm sc}$	N/A	2.6
Seed photon source energy density (erg cm^{-3})	$u_{\rm seed}$	8.3×10^{-6}	2.7×10^{-5}
Seed photon source photon energy	$\epsilon_{\rm seed}$	5×10^{-7}	5×10^{-7}
Dust torus luminosity (erg s^{-1})	$L_{\rm dust}$	7.5×10^{40}	1.9×10^{44}
Dust torus radius (cm)	$R_{\rm dust}$	6.5×10^{15}	4.1×10^{18}
Dust temperature (K)	$T_{\rm dust}$	1000	1000
Jet power in magnetic field (erg s^{-1})	$P_{\rm j,\,B}$	8.9×10^{45}	1.0×10^{47}
Jet power in electrons (erg s^{-1})	$P_{\rm j,\,e}$	2.7×10^{44}	6.6×10^{43}

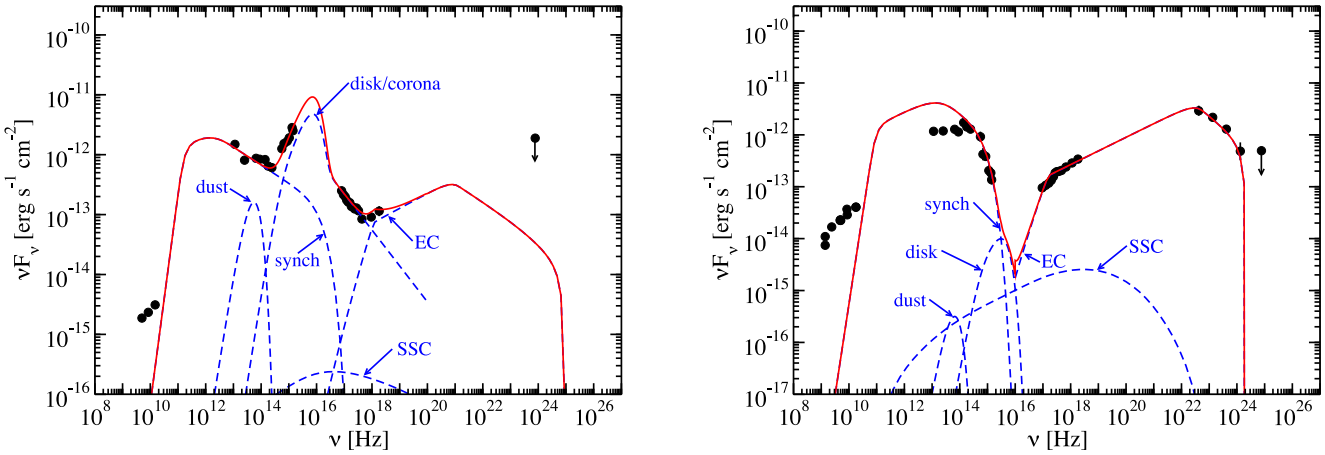

Figure 8. SED data (circles) and model fit (solid curve) of J1548+3511 (left) and PKS 2004−447 (right). The model components are shown as dashed curves. Multiwavelength data are not simultaneous.

is consistent with the value estimated by Foschini et al. (2015) on the basis of the optical spectrum, and the lack of a blue bump. This is in contrast to the modelling of PKS 2004−447 by Paliya et al. (2013) who used a much brighter dust component, which was not consistent with the disc luminosity estimated by Foschini et al. (2015). It is worth mentioning that the model parameters shown here are not unique, and other model parameters could reproduce the SED equally well. This is particularly true for J1548+3511, since without a LAT detection, its Compton component is not well constrained.

7.4 RL-NLSy1 and the young radio source population

The low BH mass and the high accretion rate commonly estimated in NLSy1 suggested that these objects may be in an early evolutionary stage (Grupe et al. 1999; Mathur 2000). Some RL-NLSy1 have been proposed to be compact steep spectrum (CSS) radio sources, on the basis of their compactness and flat/inverted spectrum which turns over at a few hundred MHz or around 1 GHz (Yuan et al. 2008). CSS are powerful radio sources whose linear size is <20 kpc. Because of their intrinsically compact size they are considered radio sources in an early evolutionary stage (see e.g. O'Dea 1998 for a review). Kinematic and radiative studies provided ages of $10^{3–5}$ yr, strongly favouring the youth scenario (see e.g. Murgia 2003; Polatidis & Conway 2003).

Many CSS sources are hosted in galaxies that recently underwent major mergers, which may have triggered the onset of the radio emission. A similar scenario was suggested by León-Tavares et al. (2014) for the RL-NLSy1 1H 0323+342. A link between NLSy1 and CSS was also proposed by Caccianiga et al. (2014)

for the RL-NLSy1 SDSS J143244.91+301435.3 on the basis of its compact size, absence of variability, and a steep radio spectrum. In this context the variable and γ-ray emitting RL-NLSy1 may be the aligned population of RL-NLSy1 where the CSS properties are hidden by dominant boosting effects. However, at least three (1H 0323+342, PMN J0948+0022, and FBQS J1644+2619) out of the six RL-NLSy1 detected in γ-rays have extended structures with linear size of 20–50 kpc (Doi et al. 2012), challenging this interpretation. Among the remaining three objects, PKS 2004−447 was suggested as a possible CSS source by Gallo et al. (2006). However, the X-ray spectra in CSS sources are typically highly obscured with column density $N_{\rm H} \gtrsim 10^{22}$ cm^{-2} (Tengstrand et al. 2009), while no absorber in addition to the Galactic one is needed for modelling the X-ray spectrum of PKS 2004−447.

The information available so far is not enough to firmly link the RL-NLSy1 to the young radio source population. Statistical multiwavelength studies on a large sample of RL-NLSy1 are required for investigating a possible connection between these subclass of radio-loud AGN.

8 CONCLUSIONS

We presented results on a multiwavelength study, from radio to γ-rays, of the RL-NLSy1 J1548+3511 and PKS 2004−447. The conclusions from this investigation can be summarized as follows.

(i) PKS 2004−447 is detected in γ-rays by LAT with an average flux between 0.1 and 100 GeV of $\sim 1.6 \times 10^{-8}$ photons cm^{-2} s^{-1}, corresponding to a luminosity of $\sim 1.6 \times 10^{45}$ erg s^{-1}, which is comparable to the values found in the other γ-ray emitting NLSy1. No strong flares have been detected so far.

(ii) J1548+3511 has not been detected in γ-rays by LAT during the first 6 yr of observations. The upper limit to the luminosity is 1.7×10^{46} erg s^{-1}.

(iii) Both sources have a clear core–jet structure on parsec scales. The majority of the radio emission comes from the core component. On arcsecond scale the radio structure is unresolved.

(iv) PKS 2004−447 shows significant variability from radio to γ-rays. In particular, at the end of 2011 and at the end of 2013 the high activity state observed in γ-rays is simultaneous to a local maximum in X-rays, UV, and optical bands, suggesting a common origin. The X-ray spectra collected by *XMM–Newton* in 2012 from 0.3 to 10 keV are fitted by a single power law. No significant X-ray photon index variability is observed in the period considered in this paper.

(v) The X-ray spectrum of J1548+3511 is well fitted by a soft component at low energy, and by a hard component above 2 keV. The X-ray flux increases of about 25 per cent in the 2 weeks between the *XMM–Newton* observations. The brightening is accompanied by a hardening of the spectrum, in particular above the energy break. This is a further indication that the emission in the high-energy part of the X-ray spectrum is dominated by the non-thermal jet emission, while a Seyfert component may be present in the low-energy part of the spectrum.

(vi) The broad-band SED of both sources can be reproduced with synchrotron, SSC, and external Compton scattering of the IR seed photons from the dust torus. The soft excess in J1548+3511 can be modelled as emission from a thermal corona. The disc luminosity of PKS 2004−447 turns out to be very weak.

(vii) The variability brightness temperature and the Doppler factor derived for both sources are similar to those found in γ-ray blazars. These characteristics together with the high radio loudness are a good proxy for the presence of relativistic jet. However, they are not good tools in the selection of γ-ray emitting NLSy1.

ACKNOWLEDGEMENTS

We thank the referee Dirk Grupe for helpful and valuable comments that improved the paper. The VLBA and VLA are operated by the US National Radio Astronomy Observatory which is a facility of the National Science Foundation operated under a cooperative agreement by Associated Universities, Inc.

The *Fermi* LAT Collaboration acknowledges generous on-going support from a number of agencies and institutes that have supported both the development and the operation of the LAT as well as scientific data analysis. These include the National Aeronautics and Space Administration and the Department of Energy in the United States, the Commissariat à l'Energie Atomique and the Centre National de la Recherche Scientifique/Institut National de Physique Nucléaire et de Physique des Particules in France, the Agenzia Spaziale Italiana and the Istituto Nazionale di Fisica Nucleare in Italy, the Ministry of Education, Culture, Sports, Science and Technology (MEXT), High Energy Accelerator Research Organization (KEK), and Japan Aerospace Exploration Agency (JAXA) in Japan, and the K. A. Wallenberg Foundation, the Swedish Research Council, and the Swedish National Space Board in Sweden. Additional support for science analysis during the operations phase is gratefully acknowledged from the Istituto Nazionale di Astrofisica in Italy and the Centre National d'Études Spatiales in France.

This research has made use of the NASA/IPAC Extragalactic Database (NED) which is operated by the JPL, California Institute of Technology, under contract with the National Aeronautics and Space Administration. This publication makes use of data products from the *Wide-field Infrared Survey Explorer* (*WISE*), which is a joint project of the University of California, Los Angeles, and the Jet Propulsion Laboratory/California Institute of Technology, and *NEOWISE*, which is a project of the Jet Propulsion Laboratory/California Institute of Technology. *WISE* and *NEOWISE* are funded by the National Aeronautics and Space Administration. This publication makes use of data products from the Two Micron All Sky Survey, which is a joint project of the University of Massachusetts and the Infrared Processing and Analysis Center/California Institute of Technology, funded by the National Aeronautics and Space Administration and the National Science Foundation.

REFERENCES

Abdo A. A. et al., 2009, ApJ, 707, L142
Abdo A. A. et al., 2010a, ApJ, 720, 912
Abdo A. A. et al., 2010b, Nature, 463, 919
Abramowski A. et al. (H.E.S.S. Collaboration), 2014, A&A, 564, A9
Acero F. et al., 2015, ApJS, 218, 23
Ackermann M. et al., 2011, ApJ, 743, 171
Ackermann M. et al., 2012, ApJS, 203, 4
Ackermann M. et al., 2015, ApJS, in press
Aharonian F. (H.E.S.S. Collaboration) et al., 2006, A&A, 457, 899
Antón S., Browne I. W. A., Marcha M. J., 2008, A&A, 490, 583
Atwood W. B. et al., 2009, ApJ, 697, 1071
Barthelmy S. D. et al., 2005, Space Sci. Rev., 120, 143
Baumgartner W. H., Tueller J., Markwardt C. B., Skinner G. K., Barthelmy S., Mushotzky R. F., Evans P. A., Gehrels N., 2013, ApJS, 207, 19
Becker R. H., White R. L., Helfand D. J., 1995, ApJ, 450, 559
Bessell M. S., Castelli F., Plez B., 1998, A&A, 333, 231
Breeveld A., Landsman W., Holland S. T., Roming P., Kuin N. P. M., Page M. J., 2011, in McEnery J. E., Racusin J. L., Gehrels N., eds, AIP Conf.

Proc. Vol. 1358, Gamma Ray Bursts 2010. Am. Inst. Phys., New York, p. 373
Burrows D. N. et al., 2005, Space Sci. Rev., 120, 165
Caccianiga A. et al., 2014, MNRAS, 441, 172
Cardelli J. A., Clayton G. C., Mathis J. S., 1989, ApJ, 345, 245
Cash W., 1979, ApJ, 228, 939
Condon J. J., Cotton W. D., Greisen E. W., Yin Q. F., Perley R. A., Taylor G. B., Broderick J. J., 1998, AJ, 115, 1693
D'Ammando F. et al., 2012, MNRAS, 426, 317
D'Ammando F. et al., 2013a, MNRAS, 433, 952
D'Ammando F. et al., 2013b, MNRAS, 436, 191
D'Ammando F. et al., 2014, MNRAS, 438, 3521
D'Ammando F. et al., 2015a, MNRAS, 446, 2456
D'Ammando F., Orienti M., Larsson J., Giroletti M., 2015b, MNRAS, 452, 520
Dermer C. D., Finke J. D., Krug H., Böttcher M., 2009, ApJ, 692, 32
Doi A., Asada K., Nagai H., 2011, ApJ, 738, 126
Doi A., Nagira H., Kawakatu N., Kino M., Nagai H., Asada K., 2012, ApJ, 760, 41
Doi A., Asada K., Fujisawa K., Nagai H., Hagiwara Y., Wajima K., Inoue M., 2013, ApJ, 765, 69
Fabian A. C. et al., 2009, Nature, 459, 540
Falcone A. D. et al., 2004, ApJ, 613, 710
Finke J. D., Dermer C. D., Böttcher M., 2008, ApJ, 686, 181
Foschini L. et al., 2012, A&A, 548, A106
Foschini L. et al., 2015, A&A, 575, A13
Gallo L. C. et al., 2006, MNRAS, 370, 245
Gehrels N. et al., 2004, ApJ, 611, 1005
Gregory P. C., Condon J. J., 1991, ApJS, 75, 1011
Grupe D., Beuermann K., Mannheim K., Thomas H.-C., 1999, A&A, 350, 805
Grupe D., Komossa S., Leighly K. M., Page K. L., 2010, ApJS, 187, 64
Hovatta T., Nieppola E., Tornikoski M., Valtaoja E., Aller M. F., Aller H. D., 2008, A&A, 485, 51
Hovatta T., Valtaoja E., Tornikoski M., Lähteenmäki A., 2009, A&A, 494, 527
Jansen F. et al., 2001, A&A, 365, L1
Kalberla P. M. W., Burton W. B., Hartmann D., Arnal E. M., Bajaja E., Morras R., Pöppel W. G. L., 2005, A&A, 440, 775
Kellermann K. I., Sramek R., Schmidt M., Shaffer D. B., Green R., 1989, AJ, 98, 1195
Komossa S., Voges W., Xu D., Mathur S., Adorf H.-M., Lemson G., Duschl W. J., Grupe D., 2006, AJ, 132, 531
Königl A., 1981, ApJ, 243, 700
Langston G. I., Heflin M. B., Conner S. R., Lehár J., Carrilli C. L., Burke B. F., 1990, ApJS, 72, 621
León-Tavares J. et al., 2014, ApJ, 795, 58
Markarian B. E., Lipovetsky V. A., Stepanian J. A., Erastova L. K., Shapovalova A. I., 1989, Soobshcheniya Spetsial'noj Astrofiz. Obser., 62, 5
Mason K. O. et al., 2001, A&A, 365, L36
Mathur S., 2000, MNRAS, 314, 17
Mattox J. R. et al., 1996, ApJ, 461, 396
Miller L., Turner T. J., Reeves J. N., Braito V., 2010, MNRAS, 408, 1928
Mirzoyan R., 2015, Astron. Telegram, 7416
Mukherjee R., 2015, Astron. Telegram, 7433
Murgia M., 2003, Publ. Astron. Soc. Aust., 20, 19
Nenkova M., Sirocky M. M., Nikutta R., Ivezić Ž., Elitzur M., 2008, ApJ, 685, 160
O'Dea C. P., 1998, PASP, 110, 493
Oshlack A. Y. K. N., Webster R. L., Whiting M. T., 2001, ApJ, 558, 578
Osterbrock D. E., Pogge R. W., 1985, ApJ, 297, 166
Paliya V. S., Stalin C. S., Shukla A., Sahayanathan S., 2013, ApJ, 768, 52
Paliya V. S., Sahayanathan S., Parker M. L., Fabian A. C., Stalin C. S., Anjum A., Pandey S. B., 2014, ApJ, 789, 143
Panessa F. et al., 2011, MNRAS, 417, 2426
Polatidis A. G., Conway J. E., 2003, Publ. Astron. Soc. Aust., 20, 69
Readhead A. C. S., 1994, ApJ, 426, 51
Richards J. L., Lister M. L., 2015, ApJ, 800, 8
Roming P. W. A. et al., 2005, Space Sci. Rev., 120, 95
Savolainen T., Homan D. C., Hovatta T., Kadler M., Kovalev Y. Y., Lister M. L., Ros E., Zensus J. A., 2010, A&A, 512, A24
Schlafly E. F., Finkbeiner D. P., 2011, ApJ, 737, 103
Steiner J. F., Narayan R., McClintock J. E., Ebisawa K., 2009, PASP, 121, 1279
Tengstrand O., Guainazzi M., Siemiginowska A., Fonseca Bonilla N., Labiano A., Worrall D. M., Grandi P., Piconcelli E., 2009, A&A, 501, 89
Wilms J., Allen A., McCray R., 2000, ApJ, 542, 914
Yuan W., Zhou H. Y., Komossa S., Dong X. B., Wang T. G., Lu H. L., Bai J. M., 2008, ApJ, 685, 801
Zhou H. et al., 2007, ApJ, 658, L13

This paper has been typeset from a TEX/LATEX file prepared by the author.